Theory for the dynamics of excited electrons in noble and transition metals

2002 J. Phys.: Condens. Matter 14 R739

(http://iopscience.iop.org/0953-8984/14/27/201)

INSTITUTE OF PHYSICS PUBLISHING JOURNAL OF PHYSICS: CONDENSED MATTER

J. Phys.: Condens. Matter **14** (2002) R739–R765 PII: S0953-8984(02)30339-4

TOPICAL REVIEW

Theory for the dynamics of excited electrons in noble and transition metals

R Knorren, G Bouzerar and K H Bennemann

Institute for Theoretical Physics, Freie Universitat Berlin, 14195 Berlin, Arnimallee 14, Germany

Received 1 November 2001, in final form 16 May 2002
Published 28 June 2002
Online at stacks.iop.org/JPhysCM/14/R739

Abstract

Using the Boltzmann equation in the random-k approximation we study in detail the dynamics of excited electrons in noble and transition metals. We present results showing the role of secondary electrons, transport and electron–phonon collisions in the hot-electron distribution, the two-photon photoemission (2PPE) current and the relaxation time and compare them to experimental data for noble and transition metals. The calculated relaxation times in Cu and Au show an unusual peak at the threshold for photoexcitation from the d band in agreement with results from 2PPE experiments. The height of the peak depends linearly on the d-hole lifetime, which can be explained by tracing the origin of the peak to Auger electrons. At zero temperature, ballistic transport of electrons strongly reduces the relaxation time of low-energy electrons in the noble metals. Taking into account elastic electron–phonon scattering, the relaxation time increases significantly with rising temperature due to the randomization of electron momenta by electron–phonon collisions. This result may explain the surprising temperature dependence of the relaxation time observed in Cu. The calculations for thin films show that the confinement of excited electrons in the film reduces the transport effect and increases the relaxation time as compared to a bulk sample. For the ferromagnetic transition metals Fe, Co and Ni, the relaxation time is strongly spin dependent and the spin-averaged relaxation time is much shorter than in the noble metals. Comparison with experimental results reveals that the magnitude and spin dependence of the relaxation time are determined by the density of states as well as the Coulomb matrix elements. It is of interest that our results shed light on the validity of the random-k approximation. This is important for extending our theory to allow for k-dependent relaxation.

(Some figures in this article are in colour only in the electronic version)

Contents

1. Introduction

Within the last decade, femtosecond pump–probe techniques have been intensively used to study the non-equilibrium dynamics of excited electrons in metallic, semiconducting and more recently high-T_c superconducting materials. Time-resolved two-photon photoemission (TR-2PPE) spectroscopy is a very efficient tool for measuring directly the time evolution of the excited-electron distribution. It provides information on different processes such as electron–electron scattering and secondary processes, electron–phonon collisions and excited-electron transport contributing to the dynamics of excited electrons. In principle, the Keldysh formalism which is an extension of the standard Green function formalism to the non-equilibrium case is well suited for describing excited electrons. Unfortunately, this is not a method which can be easily handled in the case where the band-structure is complicated. Furthermore, in such a theory it is not easy to include properly secondary-electron generation, transport and electron–phonon scattering. Such a quantum Boltzmann-equation-like treatment is a generalization of the standard Boltzmann equation in the sense that it is more suitable for strongly interacting electrons and that it properly includes quantum effects such as coherence and memory effects.

The standard Boltzmann equation can be understood as the limiting case where electrons interact only weakly with each other and can be described as free particles in between collisions. This should provide a reasonable description of the physics of excited electrons in metals at sufficiently low electron density (or equivalently in the low-laser-intensity regime). In this article, we use the standard Boltzmann equation in the random-k approximation. This means that we do not use the energy–momentum relationship for bulk crystals, but use an isotropic distribution of momenta for each energy. The random k-approximation is based on a semi-classical representation in which the electron is described as a localized wavepacket rather than as a single extended Bloch state. Furthermore, since the localized electron wavefunction can be expressed as a superposition of Bloch states, there is no direct correspondence between energy and momentum and no k-selectivity. Thus, as an input for the Boltzmann equation one retains only the integrated density of states (IDOS) over the whole Brillouin zone.

Let us discuss the appropriateness of the random-k approximation for the Boltzmann equation and the interpretation of 2PPE. 2PPE spectroscopy is based on time resolution and the dynamics of a non-equilibrium intermediate state, which makes transport and electron–electron scattering effects important. These effects can be naturally treated using the Boltzmann equation in the random-k approximation with its description of electrons as localized wavepackets rather than extended Bloch states. This behaviour of electrons is strongly supported by transport measurements [27–29], which clearly show that electrons are excited close to the surface and propagate into the bulk with approximately the Fermi velocity. In the random-k approximation, there is no distinction made for photoemission from single crystals with different surface orientations, in agreement with experimental 2PPE measurements [6], which also have not revealed clear features of k-resolution so far. Further, in contrast to assuming Bloch states with definite momentum, in the case where the electronic states contain a superposition of different momenta one can observe a photoemission current for symmetry directions where the band-structure shows a band gap. This is also supported by 2PPE experiments.

The Boltzmann equation in the random-k approximation is used to address a wide range of physical problems which can be studied using 2PPE. We discuss relaxation times of excited electrons observed in two-photon photoemission experiments in noble and transition metals. In particular, we point out the effect of secondary electrons on the relaxation time which is reflected in the photon energy dependence and the unusual peak structure of the relaxation time of copper. Furthermore, transport of photoexcited electrons out of the detection region and propagation of ballistic electrons into the bulk are discussed. We provide an explanation for the influence of electron–phonon scattering and the temperature dependence of the relaxation time observed in 2PPE. We then analyse the effect of film thickness on 2PPE. Finally, spin-dependent relaxation times in ferromagnetic transition metals are studied.

2. Theory

As mentioned above, the use of the Boltzmann equation in the random-k approximation implies (i) a semi-classical description of the electrons as localized wavepackets, (ii) that coherent effects and many-body correlations can be (in the low-laser-intensity regime) neglected and (iii) that no details of the band-structure are required except for the IDOS. The advantage of making use of the Boltzmann equation in the random-k approximation is that it will provide a very simple tool for analysing the population dynamics in non-equilibrium cases. Indeed we will show that the theory contains only a small number of parameters. The most relevant processes are included in a transparent way. Furthermore, our study allows a direct comparison with experimental measurements.

2.1. Electron–electron scattering rates

For the Boltzmann equation the transition rates due to electron–electron collisions are derived by using Fermi's golden rule. The contribution of the electron–electron collisions to the time evolution of the non-equilibrium distribution consists of two terms:

$$\left.\frac{\partial f_{E\sigma}}{\partial t}\right|^{\mathrm{e-e}} = \left.\frac{\partial f_{E\sigma}}{\partial t}\right|^{\mathrm{e-e}}_{\mathrm{out}} + \left.\frac{\partial f_{E\sigma}}{\partial t}\right|^{\mathrm{e-e}}_{\mathrm{in}}. \tag{1}$$

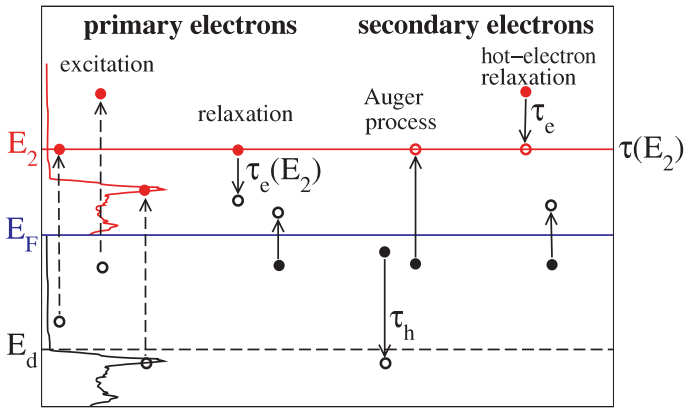

Figure 1. An illustration of secondary-electron generation.

These terms correspond respectively to scattering out of states with energy E and spin $\sigma = \uparrow, \downarrow$ and are given by

$$\left.\frac{\partial f_{E\sigma}}{\partial t}\right|_{\text{out}}^{\text{e-e}} = -f_{E\sigma}\frac{1}{2}\int_{-\infty}^{\infty} \mathrm{d}E' \{h_{E'\sigma} W(E\sigma, E'\sigma) + h_{E'\bar{\sigma}} W(E\sigma, E'\bar{\sigma})\}, \tag{2}$$

and

$$\left.\frac{\partial f_{E\sigma}}{\partial t}\right|_{\text{in}}^{\text{e-e}} = (1 - f_{E\sigma})\frac{1}{2}\int_{-\infty}^{\infty} \mathrm{d}E' \{e_{E'\sigma} W(E'\sigma, E\sigma) + e_{E'\bar{\sigma}} W(E'\bar{\sigma}, E\sigma)\}. \tag{3}$$

Here,

$$W(E\sigma, E'\sigma) = \frac{2\pi}{\hbar}\int_{-\infty}^{\infty} \mathrm{d}\varepsilon \, (e_{\varepsilon\sigma} h_{\varepsilon+\omega,\sigma} 2|M^{\uparrow\uparrow}|^2 + e_{\varepsilon\bar{\sigma}} h_{\varepsilon+\omega,\bar{\sigma}} |M^{\uparrow\downarrow}|^2), \tag{4}$$

and

$$W(E\sigma, E'\bar{\sigma}) = \frac{2\pi}{\hbar}\int_{-\infty}^{\infty} \mathrm{d}\varepsilon \, e_{\varepsilon\bar{\sigma}} h_{\varepsilon+\omega,\sigma} |M^{\uparrow\downarrow}|^2. \tag{5}$$

The quantity $e_{E\sigma} = \rho_{E\sigma} f_{E\sigma}$ is the number of electrons and $h_{E\sigma} = \rho_{E\sigma}(1 - f_{E\sigma})$ is the number of holes at energy E with spin σ. ρ denotes the density of states (DOS) and f the occupation function. The energies involved in the transition are E, E', ε and $\varepsilon + \omega$, where $\omega = E - E'$ is the energy transferred in the transition. The spin is denoted by σ and the opposite spin by $\bar{\sigma}$. The Coulomb matrix elements $|M^{\sigma\sigma'}|^2$ are averaged over momentum and energy [21, 35] and include screening effects.

If we consider a level above the Fermi level, the 'out-term' describes the relaxation of the excited electrons, whilst the 'in-term' is a source term which corresponds to the refilling of the level by highly excited electrons. This term is the so-called secondary-electron generation rate. The process is illustrated in figure 1. The secondary-electron generation has two contributions: one corresponds to the relaxation of more highly excited electrons and another, called the Auger process, describes the refilling of a hole by a cold electron (an electron below the Fermi level). The latter process is mainly controlled by the hole lifetime. As will be illustrated later, the secondary electrons are crucial for understanding the dynamics of excited electrons in noble metals. It is interesting to note that if one assumes that secondary electrons are negligible, i.e. if we keep only the out-term, then the relaxation time reduces to the lifetime which corresponds to the relaxation time approximation. In this case, it is straightforward to show that we recover

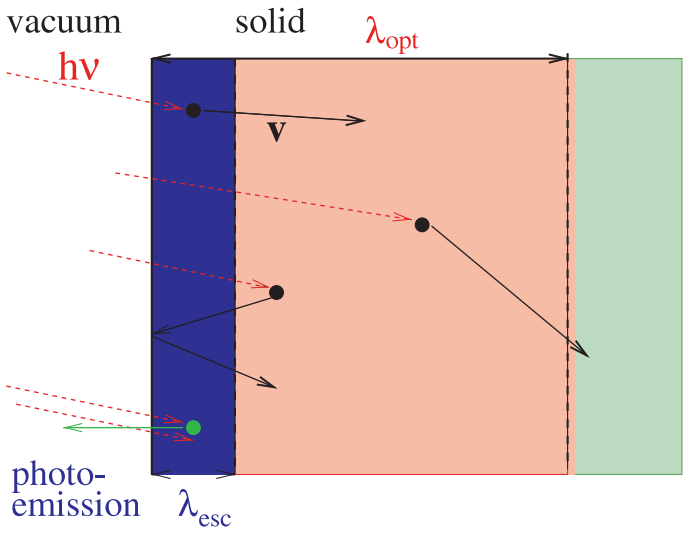

Figure 2. An illustration of the transport of excited electrons away from the surface; λ_{opt}, λ_{esc} are respectively the optical penetration depth and the escape depth.

the Fermi-liquid behaviour $\tau(E) \propto (E - E_F)^{-2}$ for the lifetime of a single excited electron [21]. The Boltzmann equation in the relaxation time approximation simplifies to

$$\left.\frac{\partial f(E\sigma)}{\partial t}\right|_{\text{out}}^{\text{e-e}} = -\frac{f(E\sigma)}{\tau_{ee}(E\sigma)}, \tag{6}$$

with the definition

$$\frac{1}{\tau_{ee}(E\sigma)} = \frac{1}{2}\int_{-\infty}^{\infty} dE' \{h_{E'\sigma} W(E\sigma, E'\sigma) + h_{E'\bar{\sigma}} W(E\sigma, E'\bar{\sigma})\} \tag{7}$$

for the inverse lifetime. The notation τ_{ee} is introduced to show that this is the single-electron lifetime due to electron–electron scattering.

2.2. *Ballistic transport*

There are several experiments providing evidence that supports the idea that a minimal theoretical model should include the transport of electrons out of the detection region. For instance, this was clearly illustrated by reflectivity measurements on Au films of varying thickness. The experiments have shown strong ballistic electron transport. The question of whether the transport is already effective over a very short timescale is still a subject of controversy among theoreticians. Let us provide some simple arguments for transport of electrons out of the detection region already influencing the dynamics of the electrons on the femtosecond timescale, illustrated by figure 2. Excited electrons are created within the optical penetration depth λ_{opt} which depends on the laser frequency. If they absorb a second photon within the escape depth λ_{esc}, they can be photoemitted. Once excited, these electrons propagate isotropically with a velocity of the order of the Fermi velocity v_F. As a consequence, an average motion of electrons into the bulk develops. The propagation of electrons parallel to the surface is not relevant, since the size of the laser spot is R_l which is of order μm—much larger than the other available length scales. Since the initial distribution of excited electrons after the pump pulse has a typical profile of the form $f(z) \propto \exp(-z/\lambda_{opt})$, where $\lambda_{opt} = 15$ nm for

a photon energy $h\nu = 3$ eV, this gives a typical transport timescale $\tau_{\rm tr} = \lambda_{\rm opt}/v_{\rm F} = 10$ fs. Hence for electronic lifetimes longer than few tens of femtoseconds, the ballistic transport will efficiently transport electrons out of the probed region on a timescale much shorter than the lifetime. This shows immediately that the transport of electrons can be seen as an additional effective decay channel which cannot be neglected. The experimental evidence for transport of electrons into the bulk provide furthers support for the description of the excited electrons as localized wavepackets, which supports the use of the Boltzmann equation. The transport can now be implemented in a very simple way, since it results from the gradient in the particle density driven by the non-uniform heating of the sample by the pump pulse. Thus, we have

$$\left.\frac{\partial f(E,z,v_z)}{\partial t}\right|^{\rm trans} = -v_z\,\nabla_z f(E,z,v_z). \tag{8}$$

In addition to the energy, E, the distribution function depends on the distance from the surface, z, and on the z-component of the velocity, v_z. One should also take into account that due to their different natures, the sp and d electrons have different velocities. Indeed due to the flatness of the d bands, which reflects the strongly localized character of d wavefunctions, one concludes that only sp electrons will participate in the transport.

2.3. Electron–phonon scattering

So far we have not discussed the role of electron–phonon collisions which are known to be crucial on the picosecond timescale, since they provide the energy transfer to the lattice and allow the return of the system to equilibrium. After about 1 ps the electrons are thermalized and the transfer of energy to the lattice starts to get effective and leads to the cooling of the electrons. This is well described and understood in the framework of the two-temperature model. But on the femtosecond timescale in which we are interested the exchange of energy between electrons and lattice via phonons is negligible and the electrons are not thermalized yet. However, if (i) sufficiently large momentum transfer is allowed and if (ii) the electron phonon scattering rate is large enough, one should expect electron–phonon collisions to have a strong effect on the nature of the electron transport. As we will see later, these two conditions are effectively fulfilled in noble metals. For example, in Cu the electron–phonon scattering time is about 30 fs, the average phonon energy $\hbar\langle\omega_{\rm ph}\rangle \approx 20$ meV and the Debye wavevector $k_{\rm D}$ is of order π/a. The random-k approximation for the electron–phonon scattering is equivalent to assuming that the electrons scatter with a bath of phonons, not keeping track of the momentum transfer and the details of the phonon spectrum. We assume that all the transitions between states of momenta k_z and k'_z are equiprobable and that the electron energy remains unchanged. With these approximations one gets [33]

$$\begin{aligned}\left.\frac{\partial f(E,z,v_z)}{\partial t}\right|^{\rm e-p} &= -\Gamma\sum[1-f(E,z,v'_z)]f(E,z,v_z)\\ &\quad+\Gamma\sum f(E,z,v'_z)[1-f(E,z,v_z)],\end{aligned} \tag{9}$$

where

$$\Gamma(T) = \frac{2\pi}{\hbar}|g|^2(2\langle n\rangle)+1)\rho(E_{\rm F}). \tag{10}$$

Γ is the electron–phonon scattering rate. The coupling function g is taken as a constant and $\langle n\rangle$ denotes the thermal average of the phonon occupation. In the limit $kT \gg \hbar\langle\omega_{\rm ph}\rangle$ the electron–phonon scattering rate reduces to the well known formula

$$\Gamma(T) = \frac{2\pi}{\hbar}\lambda kT, \tag{11}$$

where $\lambda = 2|g|^2\rho(E_{\rm F})/(\hbar\langle\omega_{\rm ph}\rangle)$ is the electron–phonon mass enhancement factor.

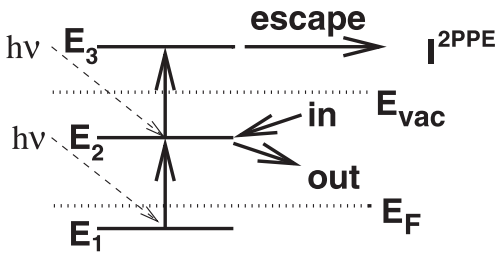

Figure 3. An illustration of the monochromatic 2PPE process with initial state E_1, intermediate state E_2 and final state E_3.

2.4. 2PPE intensity and relaxation time

We now proceed to the derivation of the two-photon photoemission current $I^{2\mathrm{PPE}}(E, \Delta t)$, where Δt is the time delay between pump and probe pulses. The 2PPE process is illustrated in figure 3. First, with the pump pulse we excite the electrons from a level E_1 below the Fermi surface to an intermediate level E_2. The time evolution of the occupation of electrons and holes is calculated within the Boltzmann equation. Then, after a time delay Δt, a second laser pulse excites the electrons from the intermediate level E_2 to a final level E_3 above the vacuum energy. The electrons can escape from this level and contribute to the measured 2PPE current. The electron in the final state is emitted into the vacuum only if it is localized in the vicinity of the surface within the escape depth λ_{esc}. The escape depth is the mean free path of electrons above the vacuum energy. The escape depth is normally energy dependent, but its dependence for electrons whose energy is close to the vacuum energy is not well known. Therefore, for simplicity we consider a constant value which is an average over energies varying between 0 and 10 eV above the vacuum. For the calculations we use an escape depth of order $\lambda_{\mathrm{esc}} \approx 1.5$ nm which is one order of magnitude smaller than λ_{opt}. Thus we get for the 2PPE current

$$I^{2\mathrm{PPE}}(E_3, \Delta t) = \int_{-\infty}^{\infty} \mathrm{d}t\, P(t - \Delta t) \int_0^{\infty} \mathrm{d}z\, \mathrm{e}^{-z/\lambda_{\mathrm{esc}}} f(E_2, z, t). \tag{12}$$

Here, a convolution of the probe laser intensity $P(t)$ with the distribution in the intermediate level is performed. The integration over z contains the restriction that only electrons within the escape depth will be detected. According to equation (12) the 2PPE current depends only on the dynamics of the intermediate level.

Now we extract the relaxation time from the 2PPE current in the same way as the experimentalists do. For a given energy, we first integrate the Boltzmann equation in the relaxation time approximation to get

$$\frac{\partial f}{\partial t} = P(t) - \frac{f}{\tau^*}. \tag{13}$$

With this we calculate the current $I^{2\mathrm{PPE}}(E_3, \Delta t)$ according to equation (12), where the integration over z is replaced by $f_{\tau^*}(t)$. The best fit of the parameter τ^* to an exponential decay of $I^{2\mathrm{PPE}}$ is taken as the relaxation time.

It is important to stress that the extracted relaxation time τ^* is not a lifetime of a single excitation, since it includes both the effect of the secondary-electron generation processes and transport, whereas τ^* refers to the population dynamics of excited states.

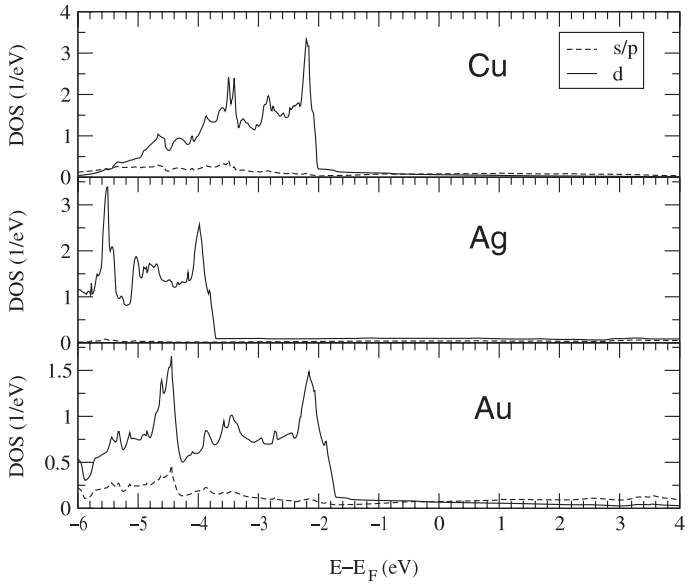

Figure 4. DOS for the noble metals [1]. Contributions from s/p and d electrons are indicated.

3. Dynamics of hot electrons in noble metals

The strong similarity of the electronic structures of Cu, Ag and Au already suggests that the lifetimes in these metals should be very similar. It is instructive to look at the DOS of Cu, Ag and Au which are shown in figure 4. One notes that the DOS is mainly of sp character in the vicinity of the Fermi energy, while it is essentially dominated by d electrons below a characteristic d-band threshold, which is about 2 eV in Cu and Au and 4 eV in Ag. While the sp electrons prevail in the vicinity of the Fermi energy, one expects the d bands to produce deviations from a free-electron-like behaviour. For large enough photon energies, excitations out of the d bands are expected to play a role.

3.1. Lifetime calculations

First, we neglect secondary electrons, ballistic transport and electron–phonon collisions. We use the random-k approximation. The Coulomb matrix element of the out-term is fitted to the value from *ab initio* calculations. It is important to stress that our theory contains only two parameters for electron–electron scattering matrix elements: one for the out-term and one for the Auger scattering rate (in-term). We use the DOS [1] which are shown in figure 4.

In figure 5 we show our calculated single-electron lifetime (solid curve) together with Fermi-liquid theory (FLT) and *ab initio* calculations. It is interesting to note that the *ab initio* calculations provide very different results from standard FLT calculations. In all cases the lifetimes from *ab initio* calculations are significantly larger than the ones calculated within FLT by a factor of 2–3. This is an illustration that the screening due to d electrons is very strong. However, one should note that in the case of Ag, where the d bands are located deeper with respect to the Fermi energy, the FLT results are closer to the *ab initio* ones, indicating a weaker screening of the d electrons than in Cu and Au. Thus, we take the *ab initio* calculations as the reference for comparison with the calculated lifetime within our theory. To get good agreement with the *ab initio* results, we find that the Coulomb matrix element should be

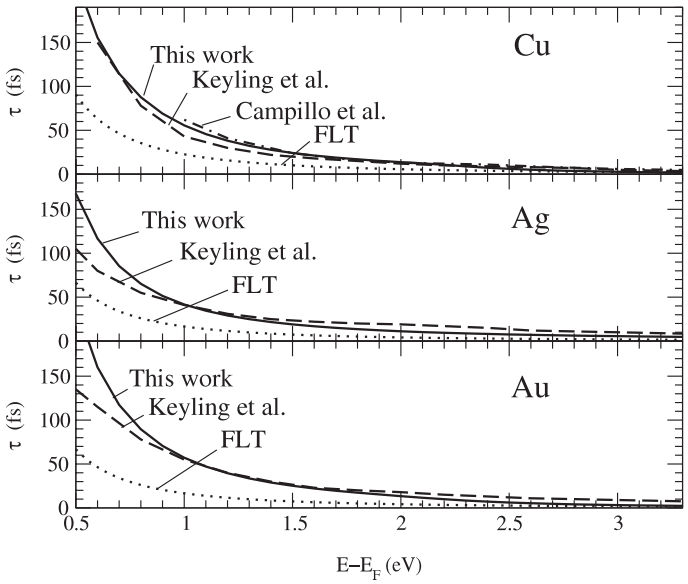

Figure 5. Single-electron lifetimes for Cu, Ag and Au calculated in the random-$\boldsymbol{k}$ approximation. Also results of FLT and of *ab initio* calculations by Campillo *et al* [2] and by Keyling *et al* [3] are shown.

$M = 0.8$ eV for Cu and Au and $M = 1.0$ eV for Ag. The larger value required for Ag agrees with the remark that the screening is somewhat weaker in Ag than in Cu and Au. It is remarkable that with only one fitting parameter our simple model provides a good agreement with the *ab initio* calculations.

3.2. Unusual behaviour of the relaxation time

Recent measurements of the relaxation time in Cu have shown an unusual peak at an energy depending linearly on the pump laser frequency. These interesting and unexpected results observed by Knoesel *et al* [5] are shown in figure 6.

It was suggested that this peak could originate from Auger electrons, i.e. secondary electrons created by the refilling of the d-band holes [5, 6]. In order to investigate the effect of Auger electrons on the relaxation time we have analysed in detail their contribution to the total hot-electron distribution and their influence on the relaxation time in the following. Note that, as we mentioned already, one should distinguish between lifetime and relaxation time, since the latter results from the non-equilibrium dynamics of the electrons and contains the effect of other contributions such as secondary-electron generation processes and transport. Previous theories neglecting secondary electrons were not able to describe this peak.

3.3. Secondary electrons and the d-hole lifetime

In figure 7(a) we show results for Cu for the distribution of hot electrons during photoexcitation at $t = 0$ (centre of the laser pulse) (a) including only primary electrons, (b) including secondary electrons without Auger electron contributions and (c) including also Auger electrons. In the case where Auger electrons are included, we have considered different d-hole lifetimes, $\tau_h = 9$, 17 and 35 fs. The distribution f_P of primary electrons shows a distinct peak at $E - E_F = 1.1$ eV and a threshold at 1.3 eV, reflecting the structure of the d band. On including secondary

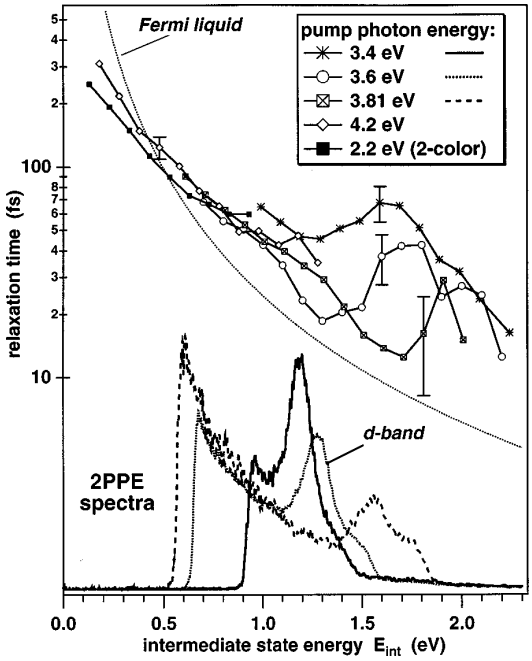

Figure 6. Relaxation times and 2PPE spectra for Cu obtained by Knoesel *et al* [5] using different pump photon energies.

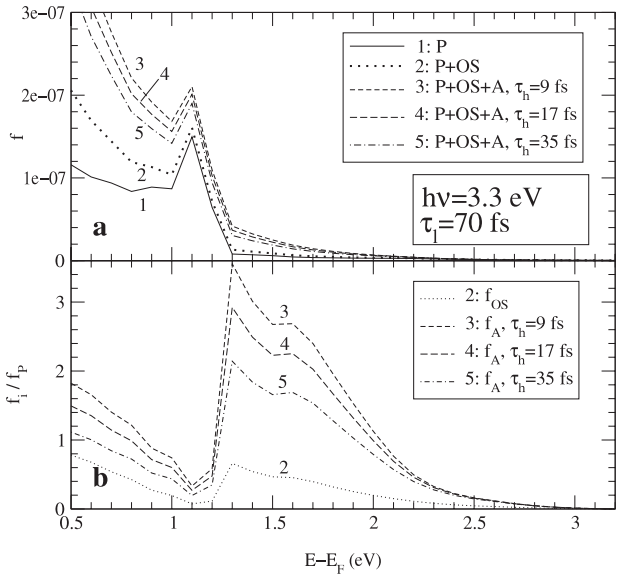

Figure 7. (a) The distribution $f(E, t = 0)$ of excited electrons during photoexcitation for different cases (1: only primary; 2: primary and other secondary; 3–5: primary, other secondary and Auger electrons for different values of the hole lifetime τ_h). (b) The ratio of the distribution of Auger (f_A) and other secondary electrons (f_{OS}) to the distribution of primary electrons (f_P). The pulse duration is $\tau_l = 70$ fs and the photon energy $h\nu = 3.3$ eV.

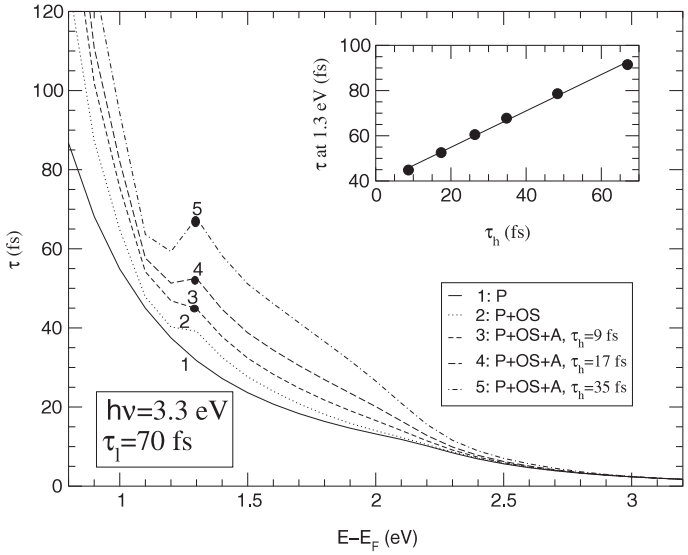

Figure 8. Effective relaxation time of excited electrons (determined by a fit to the 2PPE signal) for different hole lifetimes τ_h as a function of energy. The inset shows the relaxation time at the peak position, $E - E_F = 1.3$ eV, as a function of τ_h.

electrons, the distribution is strongly increased, especially below the peak at 1.1 eV and also above the threshold. For longer hole lifetime, fewer secondary electrons are generated: a longer d-hole lifetime corresponds to a smaller rate of scattering into d holes and therefore to fewer Auger electrons being generated in a given time.

For the analysis it is instructive to write the total hot-electron distribution as $f = f_P + f_A + f_{OS}$, where f_P, f_A and f_{OS} denote the number of primary, Auger and other secondary electrons, respectively. In figure 7(b), we show the ratios f_{OS}/f_P and f_A/f_P. Note the strong variation from 1.0 to 1.5 eV due to the variation of f_P. f_{OS}/f_P and f_A/f_P show similar shapes—with a dip at the position of the peak in f (1.1 eV) and a peak at the threshold in f (1.3 eV). These data show clearly that the Auger electron contribution largely dominates for energy between 1.2 and 2 eV.

In figure 8 the hot-electron relaxation time is shown for different cases (as in figure 7). As previously explained, the relaxation time is determined by a fit of the calculated 2PPE correlation signal $I^{2PPE}(\Delta t)$ to a function describing exponential decay. When secondary electrons are included, the relaxation time is increased with respect to τ_P and additionally a small peak appears at 1.3 eV. The enhancement with respect to the lifetime shows how important the secondary-electron cascade is. The position of the peak coincides with the threshold for excitation from the d band, in agreement with experimental results [5, 6, 36, 37]. Furthermore, it was also checked that in agreement with the experimental data its position is shifted linearly with the laser frequency.

The deviation of τ including secondary electrons from the single-electron lifetime τ_P shows a similar behaviour to the function f_S/f_P in figure 7(b). The deviation is smallest at the position of the peak in f_P (1.1 eV) and largest at the threshold for excitation from the d band (1.3 eV). Thus, in the region of the peak one observes mainly relaxation of primary electrons, while above the threshold the influence of secondary (especially Auger) electrons becomes stronger. At high energy where the secondary-electron contribution becomes negligible, the relaxation time coincides with the lifetime.

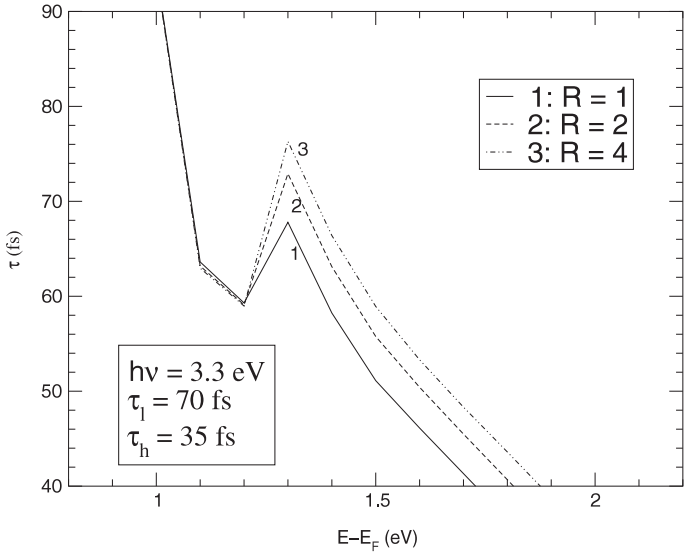

Figure 9. The dependence of the relaxation time on the ratio of optical transition matrix elements $R = |M_{\mathrm{d}\to\mathrm{s}}|^2/|M_{\mathrm{s}\to\mathrm{s}}|^2$. The pulse duration is $\tau_{\mathrm{l}} = 70$ fs, the photon energy is $h\nu = 3.3$ eV and the hole lifetime is $\tau_{\mathrm{h}} = 35$ fs.

The peak becomes more pronounced with increasing hole lifetime. For $\tau_{\mathrm{h}} = 35$ fs the height of the peak is $\Delta\tau = \tau(1.3\ \mathrm{eV}) - \tau(1.2\ \mathrm{eV}) \approx 10$ fs. This is in fair agreement with experimental results, but still somewhat too small. In different experiments on single crystals the measured height of the peak was 15–40 fs [5, 6, 36, 37]. An experiment on polycrystalline Cu has given $\Delta\tau = 17$ fs [37]. Note that the results of our theory in the random-k approximation are most suitable for comparison with measurements on polycrystalline material.

The inset of figure 8 shows the relaxation time at the threshold as a function of the d-hole lifetime. One can see that the relaxation timescales linearly with the d-hole lifetime. This shows that the d-hole lifetime may be the key factor determining the peak in the relaxation time. Its position depends only on the position of the d-band threshold and on the laser frequency.

The influence of the Auger electrons and the d-hole lifetime on the excited-electron relaxation time can be made clear with the following argument. When the holes in the d band created by the optical excitation are filled, Auger electrons are scattered into the excited level. The relaxation time observed in this level is apparently increased, since the refilling by Auger electrons occurs with a time delay with respect to the excitation of primary electrons. As a consequence, one gets a longer relaxation time. The longer the d-hole lifetime, the later (on average) the Auger electrons are scattered into the excited level and the longer the observed relaxation time. The fact that the dependence of the relaxation time on the d-hole lifetime is linear might seem surprising, since a longer d-hole lifetime implies not only a longer time delay, but also a smaller number of Auger electrons generated in a given time interval (see $f_{\mathrm{A}}/f_{\mathrm{P}}$ in figure 7(b)). However, the linear behaviour shows that the time delay (determined by the hole lifetime) is the decisive factor and that the number of Auger electrons generated does not play an important role.

In figure 9, we show the dependence of the peak on the optical transition matrix element ratio, which is another free parameter of the theory. Previously we have seen that the structure of the peak is intimately related to the photoexcitation below and above the d-band threshold. The relative intensity of excitation below and above threshold is governed by the ratio of the

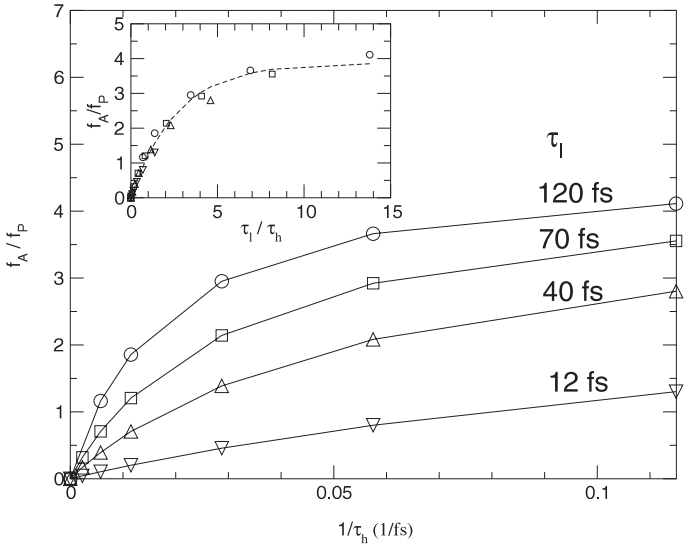

Figure 10. The ratio of the Auger to the primary electron contribution, f_A/f_P, at $E - E_F = 1.3$ eV, as a function of the inverse hole lifetime $1/\tau_h$ for different laser pulse durations τ_l. In the inset, we show f_A/f_P as a function of τ_l/τ_h. The dashed curve is a guide to the eye and indicates that the ratio f_A/f_P is controlled by τ_l/τ_h.

optical transition matrix elements for d $\rightarrow$ sp and sp $\rightarrow$ sp transitions, $R = |\mu_{ds}/\mu_{ss}|^2$. The results shown so far were obtained for equal matrix elements, $R = 1$. However, due to selection rules, one would expect $|M_{ds}|^2 > |M_{ss}|^2$. For example, for Ag, a ratio $R = 2.21$ is estimated [38], which should also be a good estimate for the magnitude of R for Cu. In figure 9 we show the relaxation times for $R = 1$, 2 and 4, using $\tau_h = 35$ fs for the hole lifetime. We find that the height of the peak, $\Delta\tau = \tau(1.3\text{ eV}) - \tau(1.2\text{ eV})$, varies significantly from 9 to 14 fs (increase by 60%) when changing R from 1 to 2. However, for a further change of R from 2 to 4, $\Delta\tau$ increases only slightly. In conclusion, for realistic values of $R = 2$ and $\tau_h = 35$ fs, we obtain for the height of the peak $\Delta\tau = 14$ fs. This is in fair agreement with experimental results for polycrystalline Cu, $\Delta\tau = 17$ fs [37]. Additionally one should mention that since in our theory there is no distinction between direct and indirect transitions, R can also be interpreted as an effective ratio including both effects. Also note that the inclusion of transport affects only the absolute magnitude of the relaxation time, but not the shape and the height of the peak.

3.4. Effect of transport: ballistic and diffusive regimes

In this section we will discuss how transport affects the dynamics of excited electrons. The importance of transport of excited electrons out of the detection region was noted in 2PPE experiments [5, 7, 30, 31]. Also, reflectivity measurements on Au films of varying thickness have revealed that a strong ballistic component of electronic transport is present [27–29]. An order-of-magnitude estimate for the transport timescale is obtained from the velocity of the electrons and the gradient of the distribution as $1/\tau_{tr} \approx v\,\partial f/\partial z$. The initial distribution is created with a spatial profile given by $f(z) \propto \exp(-z/\lambda_{opt})$, where the optical penetration depth for Cu at $h\nu = 3$ eV is $\lambda_{opt} = 15$ nm. The average transport velocity is about half of the Fermi velocity. The transport timescale is then given by $\tau_{tr} \approx 2\lambda_{opt}/v_F = 20$ fs. This shows that the transport timescale is of the order of the electronic relaxation times in noble metals.

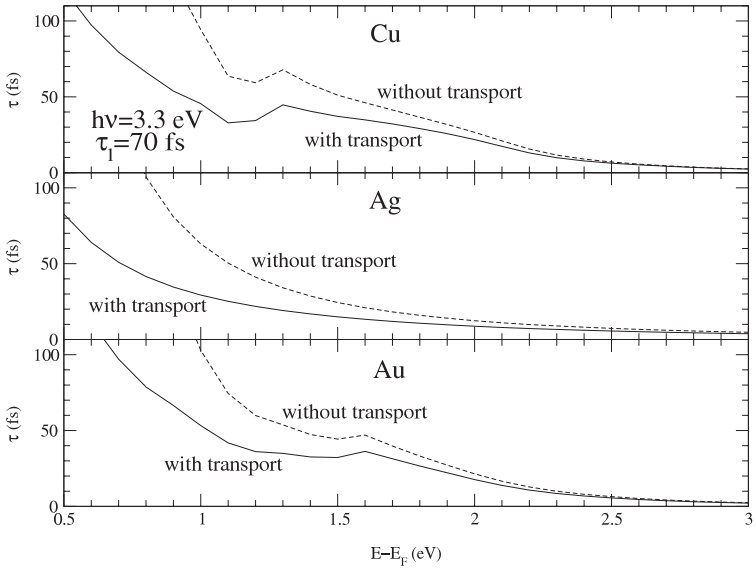

Figure 11. Effective relaxation times for Cu, Ag and Au with and without ballistic transport for bulk systems. The laser pulse duration is $\tau_l = 70$ fs and the photon energy $h\nu = 3.3$ eV. For Cu and Au, the d-hole lifetime is taken as $\tau_h = 35$ fs.

Thus one expects a significant effect of transport on the relaxation time. Transport acts like an additional 'decay' channel and reduces the relaxation time, since particles leave the detection region and penetrate into the bulk. However, elastic collisions by phonons, defects or grain boundaries can reduce the effect of transport (we consider electron–phonon collisions as elastic because the energy transfer is negligible compared to the excitation energies of the electrons). If the collision rate is high enough, transport will be less effective, since it takes place in a diffusive regime. Therefore, it is important to determine the effect of transport and its possible reduction by elastic collisions. We are going to discuss the effect of transport in two regimes determined by the rate of elastic collisions: (1) the ballistic regime, when no elastic collisions are present; (2) the diffusive regime, when the elastic collision rate is high enough to impede ballistic transport. In this section, ballistic transport will be discussed. The regime of diffusive transport will be studied in the next section in connection with the temperature dependence.

Ballistic transport of excited electrons, i.e. transport with the Fermi velocity in a collisionless regime, is expected to be present at low temperature in samples with few scattering centres such as impurities, defects or grain boundaries. Indeed a strong ballistic component of transport has been observed in reflectivity measurements on thin Au films [27–29]. Thus, ballistic transport may be important for the femtosecond dynamics of excited electrons. The case of ballistic transport in bulk samples is the simplest case which can be used to assess the maximum effect of transport on the relaxation time. All other cases, such as diffusive transport or transport in thin films, lead to a weaker effect.

In figure 11 we show results for the relaxation times in Cu, Ag and Au demonstrating ballistic transport effects. The case without transport includes secondary electrons. The effect of transport is a strong reduction of the relaxation time at low energy. This reflects that transport of electrons out of the detection region acts like an additional decay mechanism on top of electron–electron scattering. For example, at $E - E_F = 1.0$ eV the relaxation time is reduced by about 50% for all three metals. The reduction increases towards low energy and starts to

be important for relaxation times longer than about 40 fs, which corresponds to the typical transport timescale. For relaxation times much shorter than this, transport has no significant effect. The peak structure in the relaxation time of Cu and Au is qualitatively unchanged by the effect of transport. Thus, the discussion about the effect of secondary electrons in the previous section remains valid in the presence of transport.

3.5. Effect of the lattice temperature on the relaxation time

Recently an unusual temperature dependence of the relaxation time was reported [6]. It was found that the relaxation time increased with increasing lattice temperature. This is in contrast to the temperature dependence for the lifetime from FLT, which predicts a lower lifetime for a higher temperature due to the additional phase space available for electron–electron scattering. In this section, we present calculations which can provide a straightforward and simple explanation of the puzzling temperature dependence of the relaxation time. The proposed explanation is based on the influence of electron–phonon scattering on the transport of excited electrons. We have shown that ballistic transport strongly reduces the relaxation time. We argue that quasi-elastic electron–phonon collisions reduce the efficiency of transport and thereby increase the observed relaxation time.

We start by demonstrating how collisions affect the dynamics of the excited-electron distribution before discussing the temperature dependence of the relaxation time. We discuss the case of Cu and elastic collisions caused by phonons. As discussed in the theoretical part, the rate of elastic scattering by phonons is given by $\Gamma = 2\pi k_B T\lambda$, where $\lambda \approx 0.15$ is the electron–phonon mass enhancement factor in Cu [32]. We discuss the behaviour at $T = 0$ (collisionless or ballistic regime) and at $T = 300$ K ($\Gamma = 0.025$ eV or $\tau_{ep} = \hbar/\Gamma = 27$ fs).

In figure 12 we plot the average distance from the surface as a function of time after the photoexcitation. It is a measure for the penetration of excited electrons into the bulk and is defined as

$$\langle z(t)\rangle = \frac{\int_0^\infty \mathrm{d}z\, zN(z,t)}{\int_0^\infty \mathrm{d}z\, N(z,t)}, \tag{14}$$

where $N(z,t) = \int_0^\infty \mathrm{d}E\, \rho(E) f(E,z,t)$ is the average number of excited electrons at distance z and time t. Three cases corresponding to $T = 0$, 50 and 300 K are shown in the figure. For $T = 0$ (ballistic regime) we observe a linear increase of the distance with time. We get for the average velocity $\Delta\langle z\rangle/\Delta t \approx v_F/2$, where the factor $1/2$ can be understood easily by considering the average of the velocity in the z-direction. For $T = 50$ K, the propagation into the solid is slower and a deviation from the linear behaviour is observed starting at about $t = 150$ fs, which is close to the electron–phonon collision time at $T = 50$ K of about $\tau_{ep} = 170$ fs. This reflects the influence of inelastic collisions and a transition to a diffusive regime of transport. For $T = 300$ K one observes a diffusive behaviour from the start, due to the fact that the electron–phonon collision time of $\tau_{ep} = 27$ fs is shorter than the timescale over which we investigate the propagation. We illustrate this by fitting the data to $\langle z\rangle = \sqrt{D(t - t_0)}$, which is expected in the case of diffusive motion. An offset t_0 is introduced in order to take into account the finite duration of the laser pulse generating excited electrons. We get $D = 32$ nm^2 fs^{-1}, which agrees very well with the expression for the electronic diffusion coefficient $D = v_F l_e/3 = 29$ nm^2 fs^{-1}, where $l_e = v_F\tau_{e-ph}$ is the electronic mean free path. It is interesting to note that at $t = 0.5$ ps the excited electrons have already reached an average distance of 120 nm, about ten times larger than the optical penetration depth. This is in agreement with a value of 100 nm used to describe the initial spatial distribution of excited electrons in the two-temperature model [29]. Such a model does not describe the

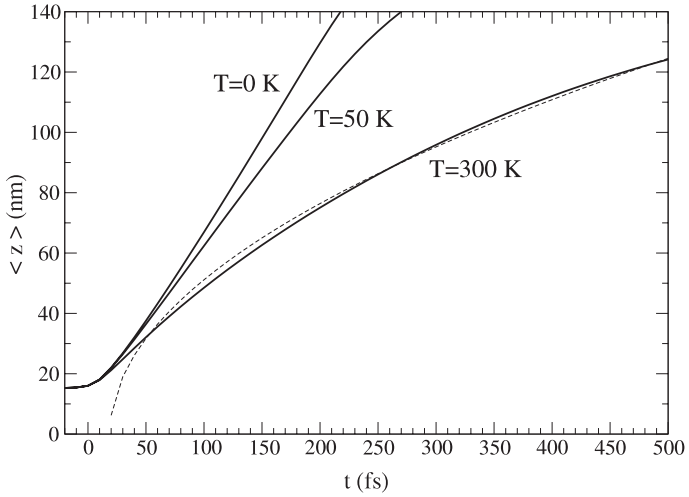

Figure 12. The average distance $\langle z \rangle$ of excited electrons from the surface after laser excitation. Note that at $T = 0$ and 50 K the transport is ballistic, while at $T = 300$ K it is diffusive due to elastic electron–phonon collisions. The dashed curve is a fit using $\langle z \rangle = \sqrt{D(t - t_0)}$. The optical penetration depth is 15 nm.

thermalization of the electron gas and starts to be valid only after $t \geqslant 0.5$ ps. Thus, one has to add $\langle z(t = 0.5 \text{ ps}) \rangle$ to the optical penetration depth. The previous figure has demonstrated that the dynamics of the excited-electron distribution is affected by elastic collisions. We have found that at higher temperature the increased electron–phonon collision rate leads to a reduction of the transport effect. In figure 13 we present theoretical results for the relaxation time for $T = 50$ and 300 K [33], together with the corresponding experimental results from [6]. First of all we note that the peak structure due to Auger electrons (see the discussion above) is not affected by transport. The change of the temperature from 50 to 300 K leads to an increase of the relaxation time. The increase is very small at high energy ($E - E_F > 1.5$ eV), but increases strongly with decreasing energy. This is understandable since collisions reduce the effect of transport, which is strong at low energy and weak at high energy. The peak structure of the relaxation time and its overall magnitude are in agreement with the experimental results. Note especially that the variation with temperature agrees excellently with the experimental results. We used $\lambda = 0.15$ from experiments to describe the electron–phonon coupling and did not introduce any arbitrary parameters in the theory.

3.6. Thin films and bulk behaviour of the relaxation time

We have found an important effect of transport in bulk samples. Although most experiments are performed on bulk samples, some data are available for films of different thicknesses. Films of varying thickness offer the opportunity to control the effect of transport. In films, the ballistic transport into the bulk of the solid is impeded by the reflection of the electrons at the substrate interface—the excited particles are confined in the film. By varying the thickness from large to small values compared to the optical penetration depth λ_{opt}, the influence of transport should be reduced from its maximum for bulk samples to zero for very thin films. We demonstrate that the film thickness can be used as a parameter to study and to control the transport effect. Further, it is shown that transport has no effect for films of thickness $d < \lambda_{opt}$, while its effect is maximal for $d \sim 10\lambda_{opt}$.

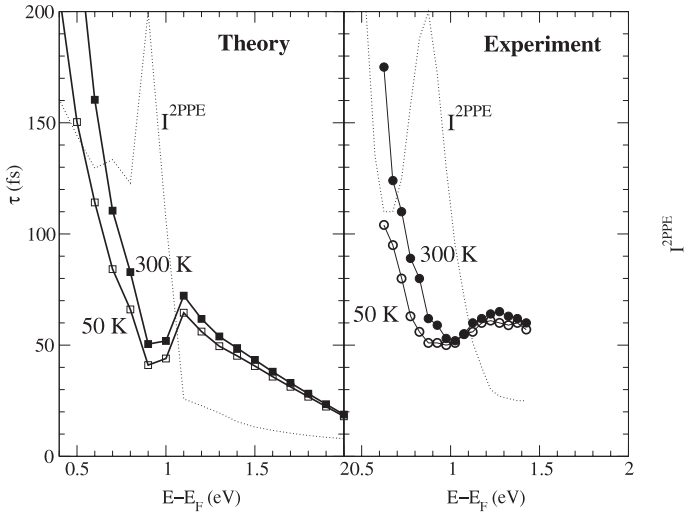

Figure 13. The temperature dependence of the relaxation time τ (experimental data for Cu(111) from [6]). The dotted curve shows the 2PPE spectrum $I^{2PPE}(E, \Delta t = 0)$ in arbitrary units. The pulse duration is 12 fs and the photon energy is 3.1 eV.

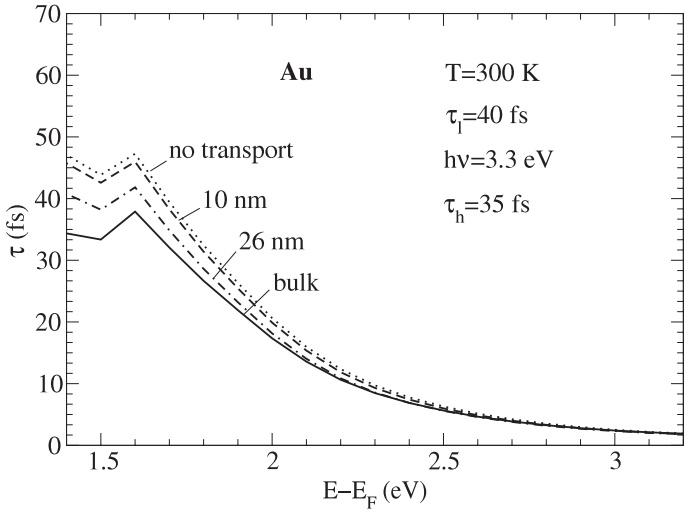

Figure 14. Relaxation times in Au films of different thicknesses. The temperature is $T = 300$ K, the laser pulse duration is $\tau_l = 40$ fs and the d-hole lifetime is taken as $\tau_h = 35$ fs.

In figure 14 we compare the relaxation time in Au films of different thicknesses. The data show a peak at 1.6 eV, which is caused by Auger electrons as discussed above. The effect of changing the film thickness from 10 to 26 nm and finally going to a bulk sample is comparable to that observed experimentally [34]. Thus for the effect of film thickness for Au, the theory gives results in reasonable agreement with the experiments.

What could cause the difference in results between Ag and Au? The first significant difference between Ag and Au is as regards the location of the d bands. However, the similarity

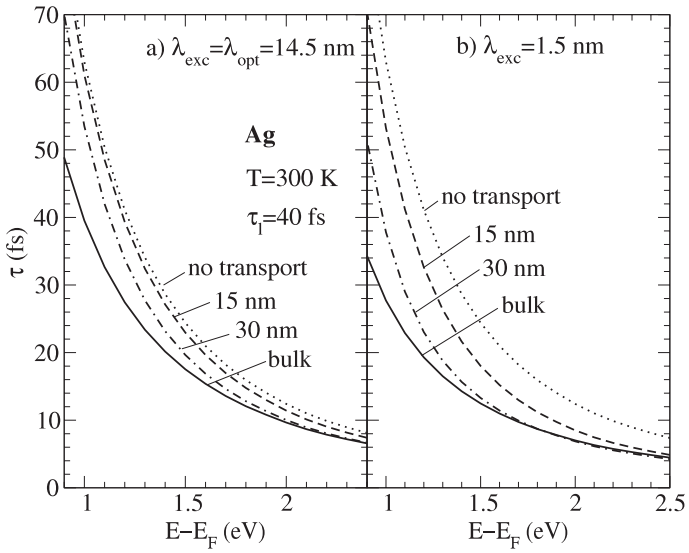

Figure 15. Relaxation times in Ag films of different thicknesses. Theoretical results for two cases: (a) excitation within the optical penetration depth $\lambda_{opt} = 14.5$ nm; (b) excitation only within $\lambda_{exc} = 1.5$ nm to simulate a surface excitation. The temperature is $T = 300$ K and the laser pulse duration is $\tau_l = 40$ fs.

of the calculated results for Au and Ag under the same conditions shows that the d bands in Au do not strongly influence the transport properties. The second difference is as regards the plasmon energy, which is around 4 eV in Ag and 8 eV in Au. The photon energy of 3.3 eV is quite close to the plasmon energy in Ag, but not that in Au. Also, the surface roughness of the Ag films used in the experiments was probably higher than that of the Au films [34]. For a rough surface, the possibility of exciting surface plasmons is enhanced. Thus there are some indications that the excitation in the Ag films may be dominated by surface plasmons. In order to test whether this leads to a stronger thickness dependence, we have calculated the relaxation time for the case of an excitation which is localized at the surface. In the calculation, we have excited electrons only within $\lambda_{exc} = 1.5$ nm from the surface. We have checked that a further decrease does not produce any changes in the relaxation time. The results for the surface excitation are shown in figure 15(b). It is seen that the difference between the 15 and 30 nm films is much stronger than in the case of a bulk excitation with $\lambda_{opt} = 14.5$ nm. This indicates that a surface excitation could indeed lead to a stronger film thickness dependence of the relaxation time.

In conclusion, the thickness dependence of the relaxation time offers the opportunity to study the effect of transport, which might depend strongly on details of the excitation mechanism. The strong difference observed in experiments between Au and Ag films of comparable thickness is unexpected. The calculations indicate that under the same conditions for the optical excitation, the thickness dependences of Au and Ag are quite similar. An excitation mainly localized at the surface due to surface plasmons in the case of Ag, but not in Au, is a possible explanation for the much stronger thickness dependence in Ag. It would be desirable to test this explanation experimentally, e.g. by using Au and Ag films of similar quality or by lowering the photon energy in order to avoid the excitation of surface plasmons.

4. Dynamics of hot electrons in transition metals

The study of the dynamical properties of the ferromagnetic transition metals Fe, Co and Ni has attracted a lot of research activity recently. They are particularly interesting because of the strong influence of the localized d electrons and because of their magnetic properties. The study of these materials is important for a better understanding of spin-dependent scattering mechanisms and in view of possible applications in magnetic recording technology and spin-electronic devices.

The influence of the unoccupied d bands in transition metals was studied in 2PPE experiments [7, 8]. It was found that as a consequence of the large phase space, the relaxation time in transition metals is shorter than that in noble metals. Analysing the spin of the photoemitted electrons, Aeschlimann *et al* [9] determined spin-dependent relaxation times in ferromagnets. The spin dependence of the mean free path was also found in a transmission experiment using thin ferromagnetic Co films [10]. A spin-dependent mean free path leads to a spin-filter effect, i.e. the preferential transmission of electrons with a particular spin orientation through ferromagnetic materials. This can be used to obtain spin-polarized electrons. The short-time dynamics in ferromagnetic transition metals has been intensively studied by optical techniques, e.g. using the magneto-optical Kerr effect or magnetization-dependent second-harmonic generation [11–14, 16–18]. Interesting magnetic effects were found—in particular a fast magnetic response to the optical perturbation. Thus, it is of great interest to study in detail the dynamics of excited electrons in ferromagnetic transition metals, in particular magnetic effects such as the spin dependence of the mean free path and of the relaxation time, and the time evolution of the spin polarization leading to a transient magnetization.

In the following section, first the single-electron lifetime and then the effective relaxation time (i.e. including secondary electrons) are discussed.

4.1. Single-electron lifetime

The single-electron lifetime is obtained when no effects due to secondary electrons or transport are taken into account. Thus the lifetime should not be directly compared to relaxation times determined in 2PPE experiments, which contain effects of secondary electrons and transport. The comparison with experiments will be made for the relaxation time presented in the next section, which includes these effects. The spin-dependent mean free path λ_σ for inelastic electron–electron scattering is related to the lifetime τ_σ via $\lambda_\sigma = \tau_\sigma v$, where v is the electronic velocity.

Due to the ferromagnetic exchange splitting, the majority and minority electrons have different DOS and also different lifetimes. The results for the lifetime are expressed in terms of the spin-averaged lifetime $\frac{1}{\tau_{\rm ave}} = \frac{1}{2}(\frac{1}{\tau_\uparrow} + \frac{1}{\tau_\downarrow})$ and of the ratio $\frac{\tau_\uparrow}{\tau_\downarrow}$ of the lifetimes.

The lifetimes are calculated using equation (7). The Coulomb matrix elements are expressed in terms of two parameters:

$$M^2 = \frac{|M^{\uparrow\uparrow}|^2 + |M^{\uparrow\downarrow}|^2}{2}, \qquad m = \frac{|M^{\uparrow\uparrow}|}{|M^{\uparrow\downarrow}|}. \tag{15}$$

Here $M^{\uparrow\uparrow}$ describes scattering between equal spins, while $M^{\uparrow\downarrow}$ is for opposite spins. M mainly influences the spin-averaged relaxation time $\tau_{\rm ave}$, while m influences the ratio $\tau_\uparrow/\tau_\downarrow$. In the calculation of the lifetime, we use the same energy-independent Coulomb matrix element $M = 0.8$ eV and $|M^{\uparrow\uparrow}/M^{\uparrow\downarrow}| = 1$ as used for Cu, where *ab initio* calculations of the lifetime are available. For the transition metals this is not the case and thus it is reasonable to use the same parameters as for Cu as a starting point. This enables direct comparison between

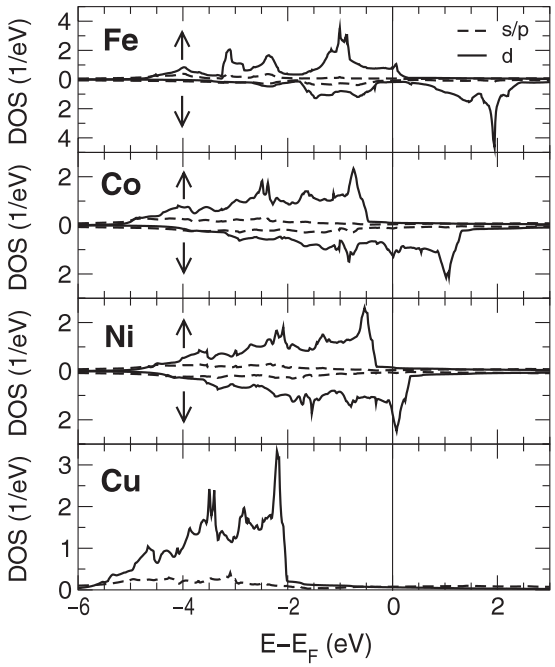

Figure 16. DOS for Fe, Co, Ni and Cu used as input for the calculation of the electron–electron scattering rates in equations (2)–(5).

the lifetimes of the different metals and a determination of the influence of the DOS. For the ferromagnetic transition metals the ratio $|M^{\uparrow\uparrow}/M^{\uparrow\downarrow}|$ has an effect on the calculated lifetime because of the different densities of states for majority and minority electrons. Due to the Pauli exclusion principle the interaction between electrons of equal spin is weaker than the one between electrons of opposite spin. Thus, one expects $|M^{\uparrow\uparrow}/M^{\uparrow\downarrow}| < 1$.

We first calculate the lifetime of Ni, Co and Fe using equal Coulomb matrix elements. In this case, the calculated results can be understood only on the basis of the different DOS shown in figure 16 and used as input for the calculation. The influence of the DOS on the single-electron lifetime is seen in equation (2) for the scattering rate expression. The scattering rate, the inverse of the lifetime, is proportional to an integral over a combination of terms which are all products of three factors of the DOS. The first factor represents the free states available for the relaxation of the initial electron, the second factor represents the occupied states containing possible scattering partners for the electron–electron collision and the third factor stands for the unoccupied state into which the second electron is scattered during the transition. Due to the integration over energy, even strong features in the DOS appear only as weak structures in the lifetime.

In figure 17(a) we show the lifetimes of Ni, Co and Fe. When comparing the single-electron lifetime of Cu with that for the transition metals, one can see that Cu has a much longer lifetime than the other metals. This is due to the small total DOS close to the Fermi energy. In Cu, the d bands are located about 2 eV below the Fermi energy and there is only a very small total DOS close to the Fermi energy (figure 16). The small d DOS close to the Fermi energy is due to hybridization with sp-like states.

In Ni with one electron fewer than Cu, the d bands move closer to the Fermi energy. Furthermore, the d bands are split into a minority spin and a majority spin band and a small

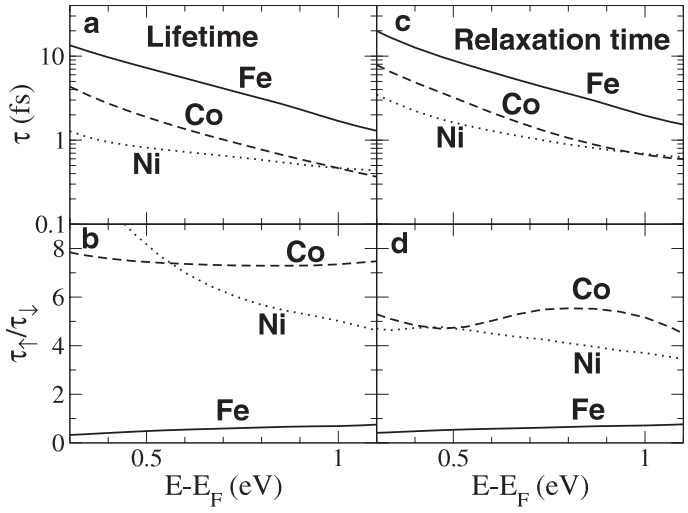

Figure 17. (a) The spin-averaged single-electron lifetime τ, (b) the ratio $\tau_\uparrow/\tau_\downarrow$ of the majority and minority lifetimes, (c) the spin-averaged relaxation time (including effects of secondary electrons), (d) the ratio $\tau_\uparrow/\tau_\downarrow$ of the majority and minority relaxation times. For the Coulomb matrix elements we use $M = 0.8$ eV and $M^{\uparrow\uparrow}/M^{\uparrow\downarrow} = 1$.

portion of the minority d band is unoccupied, extending up to about 0.4 eV above the Fermi energy (figure 16). Due to the pronounced peak at the upper edge of the d-band DOS, the minority DOS close to the Fermi energy is extremely large. This leads to a large phase space for electron–electron scattering at low energy. Thus at low energy (below $E - E_F = 1$ eV) Ni has the smallest calculated single-electron lifetime among the four elements.

Co, with one electron fewer than Ni, has an even larger portion of unoccupied minority DOS, extending up to about 1.2 eV above the Fermi energy. Although the total number of unoccupied states is higher in Co than in Ni, the minority DOS at the Fermi energy is lower in Co. Thus at low energy (below 1 eV), Co has less phase space for electron–electron scattering and the calculated lifetime is longer than in Ni. With increasing energy, more and more unoccupied states become available in Co, so above 1 eV, the calculated single-electron lifetime in Co becomes shorter than that in Ni.

In Fe, again with one electron fewer compared to Co, the unoccupied minority DOS extends up to 2.4 eV above the Fermi energy, and even the majority DOS has a small unoccupied fraction. The minority DOS at the Fermi energy in Fe is lower than in Co and in Ni, so Fe has the smallest phase space and the longest calculated lifetime at low energy. At higher energy (above 3 eV), all of the unoccupied d states in Fe are available for a transition and one calculates $\tau_{Fe} < \tau_{Co} < \tau_{Ni}$.

In conclusion, at low energy (below $E - E_F = 1$ eV) the lifetime is governed by the DOS close to E_F. Our theory with equal M for the different metals predicts $\tau_{Ni} < \tau_{Co} < \tau_{Fe}$. This trend changes for Co and Ni above 1 eV. Then we get $\tau_{Co} < \tau_{Ni}$. At high energy (above 3 eV) the lifetime is governed by the total number of free states above E_F, and this leads to $\tau_{Fe} < \tau_{Co} < \tau_{Ni}$. This relation is also observed in transmission experiments above the vacuum energy for electrons with energies above $E - E_F = 5$ eV [19, 20].

In figure 17(b) the ratio of majority to minority single-electron lifetime $\tau_\uparrow/\tau_\downarrow$ is shown. The results can be understood by using equation (7) for τ_σ. One can already get a good idea of the behaviour of τ_σ if one considers only the first factor of the DOS which describes the

phase space available for the relaxation of the excited electron. In this case the scattering rate $1/\tau(E,\sigma)$ is proportional to the integral over the unoccupied states of spin σ from the Fermi energy up to energy E.

In figure 17(b) the lifetime ratio for Ni decreases from $\tau_\uparrow/\tau_\downarrow = 9.5$ at $E - E_F = 0.4$ eV to $\tau_\uparrow/\tau_\downarrow = 4$ at $E - E_F = 1.3$ eV and then slowly decreases further to 2.5 at 3 eV. The large ratio at low energy is due to the high minority DOS which extends up to 0.4 eV above E_F. The strong decrease of the lifetime ratio with energy is due to the fact that above 0.4 eV there are no more unoccupied minority d states. The additional phase space gained by going to higher energy is equal for minority and majority electrons. Thus the relative weight of the high minority DOS close to E_F gets smaller and consequently the lifetime ratio gets smaller.

For Co, the lifetime ratio is nearly constant with a value $\tau_\uparrow/\tau_\downarrow = 7.5$ up to 1 eV. This is understandable in view of the high and nearly constant ratio of minority to majority DOS at low energy. Since the DOS is approximately constant up to 1 eV, the ratio of the lifetimes is given by $\tau_\uparrow/\tau_\downarrow = \rho_\downarrow/\rho_\uparrow$. At 1 eV, there is a small increase in the ratio which reflects the peak in the minority DOS. Again, the strong peak in the DOS appears only as a weak structure in τ due to the integration over energy. Above 1.3 eV, the ratio slowly decreases for the same reason as in Ni: the minority and majority DOS are almost equal and the phase space gained by increasing the energy is the same for majority and minority states.

The case of Fe is interesting, since it is different from those of Ni and Co. The ratio increases from $\tau_\uparrow/\tau_\downarrow = 0.5$–1 for excitation energies between $E - E_F = 0.5$ and 1.3 eV. Thus, at low energy, majority electrons have a shorter lifetime than minority electrons. This results from the unoccupied portion of the majority DOS above the Fermi energy, which leads to a larger phase space for the relaxation of majority electrons and therefore to $\tau_\uparrow < \tau_\downarrow$. The ratio is equal to 1 when the integral over unoccupied states becomes the same for minority and majority electrons. This happens around 1.3 eV. Above 1.3 eV the minority lifetime gets shorter due to there being more and more unoccupied minority states, leading to $\tau_\uparrow/\tau_\downarrow > 1$ and a strong increase towards higher energy.

4.2. Effective relaxation time

The effective relaxation time is different from the single-electron lifetime, since it includes the effects of secondary electrons. Note that transport effects have been neglected here in view of the fact that they cause only minor changes in the relaxation time of the transition metals [21]. The reason is that the typical transport timescale of about 60 fs is much longer than the electronic relaxation times in the transition metals. However, secondary-electron effects are important and cannot be neglected. As was shown in the case of the noble metals, the generation of secondary electrons leads to the observation of a longer relaxation time, especially at low energy. The laser pulse excites electrons with energies up to $h\nu$. The most energetic electrons relax very quickly, generating secondary electrons at lower energy as dictated by energy conservation. The experimental 2PPE spectra also reveal that at low energy many secondary electrons are present [9]. Thus, when analysing the relaxation of electrons in levels of low energy, it is absolutely necessary to include the effects of the secondary-electron cascade.

In the following section we will first calculate the relaxation time including secondary electrons and analyse their effect, using the same parameters for the Coulomb matrix elements as in the calculation of the lifetime; then we will compare with 2PPE experiments and discuss the influence of different Coulomb matrix elements.

For comparison with experimental results, we use the same values as in the experiments, $h\nu = 3.0$ eV and $\tau_l = 40$ fs [9, 21]. Due to the fact that the relaxation time is obtained from a fitting procedure, the lower limit and the accuracy of the calculated relaxation time are about 0.5 fs.

In figure 17(c) we show the spin-averaged relaxation time to be compared with the single-electron lifetime from figure 17(a). The inclusion of secondary electrons leads to an increase of the relaxation time by a factor of about 2 for Ni and Co and about 1.2 for Fe as compared to the corresponding single-electron lifetime. The increase is almost independent of energy, although it is slightly stronger at lower energy. The increase in the relaxation time is stronger for Ni and Co and weaker for Fe. This can be explained by the fact that the inclusion of secondary electrons leads to a coupling between majority and minority electron populations via electron–electron scattering. Relaxing minority electrons can excite majority electrons and vice versa. In Ni and Co the single-electron lifetime of minority electrons is much shorter than that of majority electrons. However, when including secondary electrons, longer-living majority electrons will continue to excite minority electrons after the shorter-lived primary minority electrons have relaxed. The effective minority electron relaxation time as well as the spin-averaged relaxation time become longer. In Fe the effect is weaker, since the difference between $\tau_\uparrow$ and $\tau_\downarrow$ is small. However, the trends among the calculated relaxation times of the transition metals, particularly the relation $\tau_{\mathrm{Ni}} < \tau_{\mathrm{Co}} < \tau_{\mathrm{Fe}}$ at $E - E_{\mathrm{F}} < 1$ eV, are unchanged when secondary electrons are included.

In figure 17(d) we show the ratio $\tau_\uparrow/\tau_\downarrow$ for the effective relaxation time of the photoexcited distribution to be compared with the value for the single-electron lifetime from figure 17(b). For Ni the ratio is reduced to $\tau_\uparrow/\tau_\downarrow = 3.5$–5, for Co to $\tau_\uparrow/\tau_\downarrow = 4.5$–5.5. The strong reduction of the ratio $\tau_\uparrow/\tau_\downarrow$ in Ni and Co can again be understood in view of the large spin dependence of the single-electron lifetime and the coupling between majority and minority electrons induced by the generation of secondary electrons. For Fe the ratio is nearly unchanged, $\tau_\uparrow/\tau_\downarrow = 0.5$–1, because the lifetimes of minority and majority electrons are comparable and the coupling between them does not lead to a strong change in the relaxation time. The strong structure in the case of Co is due to small variations in the minority relaxation time, to which the ratio $\tau_\uparrow/\tau_\downarrow$ is very sensitive. This might however be a calculational problem, since $\tau_\downarrow$ is very small already at 1 eV and cannot be determined very accurately.

After discussing the influence of secondary electrons, we compare experimental and theoretical results for the spin-averaged relaxation time τ_{ave} and the ratio $\tau_\uparrow/\tau_\downarrow$ of majority and minority relaxation times in figures 18 and 19. This comparison is used to determine the effect of the matrix elements on τ_{ave} and $\tau_\uparrow/\tau_\downarrow$. For the Coulomb matrix elements we use the two parameters M and m; see equation (15).

First, the results calculated with $M = 0.8$ eV for all the transition metals are shown by the curves a in figures 18 and 19. The differences in calculated relaxation time between Fe, Co, Ni and Cu are then only due to the different DOS used as input for the calculations. Note that the calculated relaxation time is smaller than the experimental one in Co and Ni, while it is larger in Fe. The calculated ratio $\tau_\uparrow/\tau_\downarrow$ is larger for Co and Ni than the experimental one, but it is smaller for Fe.

Secondly, as curves b, we show the results of calculations using again $M = 0.8$ eV, but the reduced value $m = 0.5$. Due to the Pauli exclusion principle the matrix element $M^{\uparrow\uparrow}$ for scattering between parallel spins contains the effect of exchange (for details see the appendix of [21]). Thus one expects the matrix element $M^{\uparrow\uparrow}$ for parallel spins to be smaller than $M^{\uparrow\downarrow}$ for antiparallel spins, since electrons with parallel spins avoid each other due to the Pauli exclusion principle [22]. A value $m < 1$ is further justified by the result of a calculation which indicates that the effect of exchange, which is contained in the matrix element $M^{\uparrow\uparrow}$, increases the lifetime for a free-electron gas at metallic densities by a factor of 1.7 [23]. As a consequence of using $m = 0.5$ in the calculation, the ratio $\tau_\uparrow/\tau_\downarrow$ in figure 19 is strongly reduced in Co and Ni, while it is increased in Fe, which leads to satisfactory agreement for $\tau_\uparrow/\tau_\downarrow$ between experimental and theoretical results. Note also that there is a considerable scatter in the experimental data, and

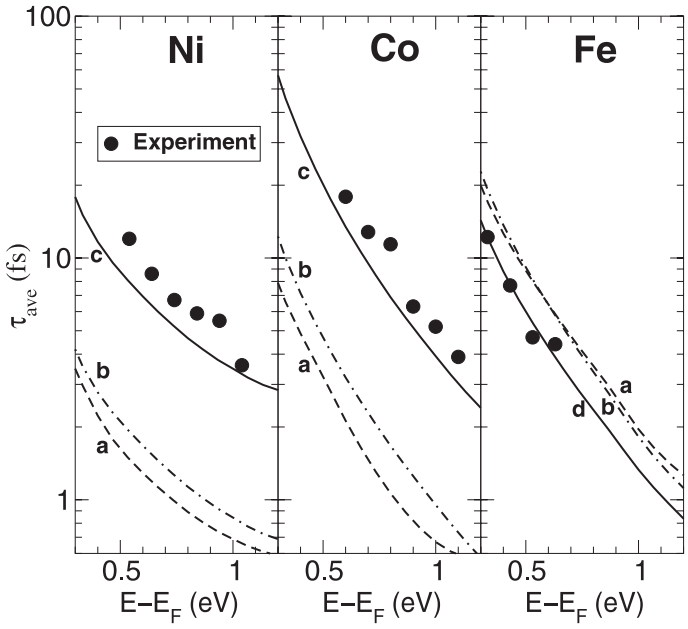

Figure 18. The spin-averaged effective relaxation time for a pulse with 40 fs duration and 3.0 eV photon energy. For the Coulomb matrix elements, we use (a) $M = 0.8$ eV, $m = M^{\uparrow\uparrow}/M^{\uparrow\downarrow} = 1$, (b) $M = 0.8$ eV, $m = 0.5$, (c) $M = 0.4$ eV, $m = 0.5$, (d) $M = 1.0$ eV, $m = 0.5$.

the error bars might actually be larger than shown in the figures. The spin-averaged relaxation time in figure 18 is not strongly affected by the value of m.

Thirdly, we take into account different Coulomb matrix elements M for the various metals, while we still use $m = 0.5$. The results are given by the curves c and d in figures 18 and 19. For Co and Ni we use $M = 0.4$ eV, while for Fe we take $M = 1.0$ eV. In the case of Cu we use $M = 0.8$ eV. The use of these values for M leads to reasonable agreement between theoretical and experimental results for both spin-averaged relaxation times in figure 18. The ratio $\tau_\uparrow/\tau_\downarrow$ in figure 19 is almost unchanged on changing M. Thus in the transition metals, in addition to the DOS, the Coulomb matrix elements play an important role in the relaxation time.

The Coulomb matrix elements for Fe, Co, Ni and Cu are different due to the influence of the d electrons. Note that while for isolated atoms Coulomb matrix elements do not vary much from Cu to Fe [24], for solids the band character, the position of the d band and the screening of d electrons are expected to change this. The screened Coulomb matrix elements are influenced by d electrons in two ways:

(1) d-electron wavefunctions are more localized than sp-electron wavefunctions, leading to smaller Coulomb matrix elements for transitions involving d states;
(2) the d electrons contribute to the screening of the Coulomb potential, leading to smaller Coulomb matrix elements if more d electrons are present.

The strong localization of d electrons leads to smaller overlap with sp-electron wavefunctions and therefore to smaller transition matrix elements when sp $\rightarrow$ d transitions are involved as compared to matrix elements involving sp $\rightarrow$ sp transitions. The d-electron wavefunctions in the solid get more localized from Fe to Cu. Thus one expects the matrix elements for transition metals, which are strongly influenced by d electrons, to be smaller than those for noble metals, which are mainly due to sp electrons. This explains the smaller matrix

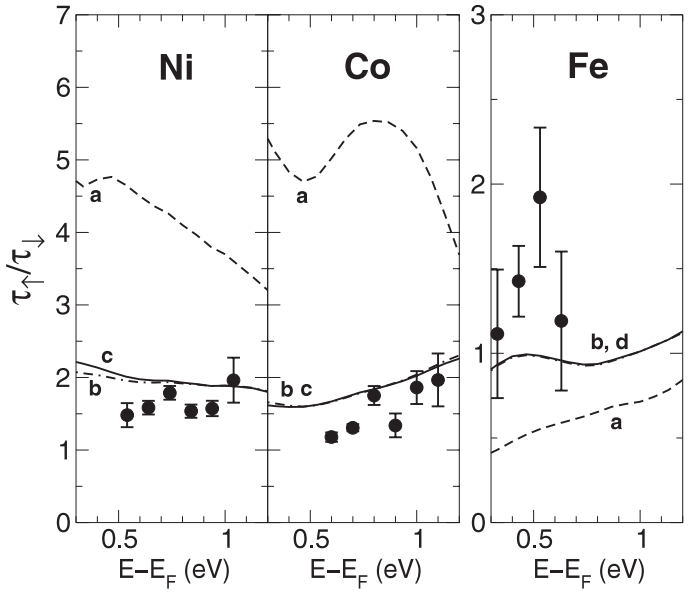

Figure 19. The ratio $\tau_\uparrow/\tau_\downarrow$ of the effective relaxation time for a pulse with 40 fs duration and 3.0 eV photon energy. For the Coulomb matrix elements, we use (a) $M = 0.8$ eV, $m = M^{\uparrow\uparrow}/M^{\uparrow\downarrow} = 1$, (b) $M = 0.8$ eV, $m = 0.5$, (c) $M = 0.4$ eV, $m = 0.5$, (d) $M = 1.0$ eV, $m = 0.5$.

elements for Co and Ni compared with Cu, but would also suggest smaller matrix elements for Fe. The argument for smaller matrix elements for Co and Ni is in accordance with a recent study by Zarate *et al* [25], which indicates that Coulomb matrix elements are smaller when more d wavefunctions are involved in the transition.

The additional screening of d electrons is contained in the dielectric function $\varepsilon(|\boldsymbol{r}-\boldsymbol{r}'|, \omega)$, where ω is the energy transferred in the transition. For small ω, d electrons close to the Fermi energy contribute mainly to screening. In the static limit ($\omega \to 0$), the Lindhard dielectric function for a free-electron gas reduces to $\varepsilon(q) = 1 + k_0^2/q^2$ with the result that the screened Coulomb interaction in real space takes the form $V(r) = \frac{e^2}{r}\mathrm{e}^{-k_0 r}$. In the Thomas–Fermi approximation, the screening wavevector is directly related to the DOS at the Fermi level [26], $k_0 = 4\pi e^2 \rho(E_\mathrm{F})$. In the case of transition metals, the expressions are not strictly valid because d electrons are not free-electron-like. Although the quantitative contribution of d electrons to screening is not well known, qualitatively it is clear that a higher DOS near the Fermi level leads to stronger screening. However, for larger energy transfer ω, electrons further away from the Fermi energy also contribute to screening. Then ultimately the total number of d electrons influences the screening. This could be why Fe, which has fewer d electrons, has a larger Coulomb matrix element than Co, Ni and Cu. The simple argument about the screening by d electrons is in line with *ab initio* calculations. The influence of the d electrons on screening was recently investigated in *ab initio* calculations of the lifetimes in Cu [2, 4] and in Au and Ag [3]. It was found that in Cu, the d bands lying 2 eV below E_F have a very strong influence on the screening properties and cause an increase of the lifetime by a factor of 2–3.

In conclusion, the relaxation times in transition metals are influenced both by the DOS and the Coulomb matrix elements. The latter are sensitively affected by the localization of the wavefunction and the screening properties. *Ab initio* calculations using realistic wavefunctions are required for a reliable estimate of their magnitude. Our results obtained by comparison

with measured relaxation times in transition metals indicate that $M = 0.4$ eV for Co and Ni and $M = 1.0$ eV for Fe. For Cu, we used $M = 0.8$ eV. Thus there seems to be no simple trend for the matrix elements among the 3d metals.

5. Conclusions

We have presented a theory for the ultrafast dynamics of excited electrons in metals including effects of the optical excitation pulse, inelastic electron–electron scattering, ballistic transport and elastic electron–phonon collisions. We have found that the calculated relaxation time reflects the interplay of the optical excitation, excited-electron relaxation, secondary-electron generation, ballistic transport of electrons out of the detection region and elastic electron–phonon collisions. Thus our theory has shown that 2PPE can be used to study a wide range of ultrafast dynamical processes in solids and has helped to identify the influence of the different mechanisms on the relaxation time measured in 2PPE experiments.

For the noble metals Cu, Ag and Au, the relaxation time obtained from $I^{2\mathrm{PPE}}(E, \Delta t)$ including the effect of the photoexcitation and of the secondary electrons is longer than the single-electron lifetime, indicating that secondary electrons have a strong influence on the relaxation time. The calculated relaxation times in Cu and Au show a peak at the threshold for photoexcitation from the d band as found by 2PPE experiments. For Cu, the position and structure of the peak are in fair agreement with the experimental results. The relaxation time at the peak position depends linearly on the d-hole lifetime τ_{h}. Using $\tau_{\mathrm{h}} = 35$ fs and $R = |M_{\mathrm{ds}}/M_{\mathrm{ss}}|^2 = 2$ for the ratio of the optical matrix elements for d $\rightarrow$ sp and sp $\rightarrow$ sp transitions, we obtain for the height of the peak $\Delta\tau = 14$ fs, in good agreement with the experimental results for a polycrystalline sample, $\Delta\tau = 17$ fs.

It was shown that the effect of ballistic transport of excited electrons out of the detection region strongly reduces the relaxation time in the noble metals at low energy, while it is nearly unchanged at higher energy.

The influence of elastic electron–phonon collisions changes the nature of the transport from ballistic at zero temperature to diffusive at room temperature. As a consequence, the relaxation time increases significantly with increasing temperature. Using the electron–phonon scattering rate from the literature, we obtain excellent agreement with experimental results for the temperature dependence of the relaxation time in Cu.

The film thickness dependence of the relaxation time was investigated. For film thickness $d < 100$ nm, the confinement of excited electrons in the film reduces the transport effect and increases the relaxation time compared to the results for a bulk sample. Our results indicate that films of varying thickness can be used to determine the transport effect by means of 2PPE, analogously to studies by optical techniques. The study of thin films by means of 2PPE has only begun, and the quantitative influence of the transport effect in films is still not settled. A systematic study can offer detailed information about the transport of excited electrons.

For the ferromagnetic transition metals Fe, Co and Ni, we calculated spin-dependent single-electron lifetimes. Due to the high d-band DOS, the spin-averaged lifetimes are much shorter than in the noble metals. The relaxation time from $I^{2\mathrm{PPE}}(E, \Delta t)$ including effects of secondary electrons is longer than the lifetime, and the ratio $\tau_\uparrow/\tau_\downarrow$ is reduced due to the coupling between minority and majority electrons caused by the secondary-electron cascade. In connection with this observation, a study of the time evolution of the spin polarization as a function of energy by means of 2PPE would be very interesting. This can provide detailed information about the transient magnetization in the excited levels, which can be related to the results using magneto-optical techniques for the study of the ultrafast magnetic dynamics.

When comparing the calculated spin-averaged relaxation times for the transition metals with experimental results from 2PPE studies, fair agreement is found when we use for the

Coulomb matrix elements $M_{\mathrm{Co}} \simeq M_{\mathrm{Ni}} < M_{\mathrm{Fe}}$. The different matrix elements reveal that the exact nature of the electronic wavefunctions and the influence of screening play important roles. For the transition metals, a detailed study of the Coulomb matrix elements by means of *ab initio* calculations is desirable in order to clarify their magnitude and spin dependence.

In the future, extensions of the theory which permit a k-selective analysis of 2PPE, k-dependent relaxation with lifetimes $\tau_{k,\sigma}$, non-equilibrium studies relating to strong laser intensities and temperature effects due to $T_{\mathrm{el}}(t)$ and $T_{\mathrm{el}} \neq T_{\mathrm{latt}}$ would be of interest. The important Coulomb matrix elements M and their screening should be calculated directly. Also, quantum interference effects should be included (see [6]).

References

[1] Densities of states were calculated by the FLAPW band-structure program WIEN95 and were provided to us by
Dewitz J 1998 private communication
[2] Campillo I, Pitarke J M, Rubio A, Zarate E and Echenique P M 1999 *Phys. Rev. Lett.* **83** 2230
[3] Keyling R, Schöne W D and Ekardt W 2000 *Phys. Rev.* B **61** 1670
[4] Schöne W D, Keyling R, Bandic M and Ekardt W 1999 *Phys. Rev.* B **60** 8616
[5] Knoesel E, Hotzel A and Wolf M 1998 *Phys. Rev.* B **57** 12 812
[6] Petek H, Nagano H and Ogawa S 1999 *Appl. Phys.* B **68** 369
[7] Aeschlimann M, Bauer M and Pawlik S 1996 *Chem. Phys.* **205** 127
[8] Knoesel E 1997 *PhD Thesis* Freie Universität, Berlin
[9] Aeschlimann M, Bauer M, Pawlik S, Weber W, Burgermeister R, Oberli D and Siegmann H C 1997 *Phys. Rev. Lett.* **79** 5158
[10] Oberli D, Burgermeister R, Riesen S, Weber W and Siegmann H C 1998 *Phys. Rev. Lett.* **81** 4228
[11] Beaurepaire E, Merle J-C, Daunois A and Bigot J-Y 1996 *Phys. Rev. Lett.* **76** 4250
[12] Hohlfeld J, Matthias E, Knorren R and Bennemann K H 1997 *Phys. Rev. Lett.* **78** 4861
[13] Hohlfeld J, Güdde J, Conrad U, Dühr O, Korn G and Matthias E 1999 *Appl. Phys.* B **68** 505
[14] Conrad U, Güdde J, Jähnke V and Matthias E 1999 *Appl. Phys.* B **68** 511
[15] Scholl A, Baumgarten L, Jacquemin R and Eberhardt W 1997 *Phys. Rev. Lett.* **79** 5146
[16] Güdde J, Conrad U, Jähnke V, Hohlfeld J and Matthias E 1999 *Phys. Rev.* B **59** R6608
[17] Knorren R and Bennemann K H 1999 *Appl. Phys.* B **68** 501
[18] Hübner W and Zhang G P 1998 *Phys. Rev.* B **58** R5920
[19] Siegmann H C 1992 *J. Phys.: Condens. Matter* **4** 8395
[20] Siegmann H C 1994 *Surf. Sci.* **307–9** 1076
[21] Knorren R, Bennemann K H, Burgermeister R and Aeschlimann M 2000 *Phys. Rev.* B **61** 9427
[22] Friedel J 1969 *Physics of Metals* vol 1, ed J M Ziman (Cambridge: Cambridge University Press) ch 8
[23] Ritchie R H and Ashley J C 1965 *J. Phys. Chem. Solids* **25** 1689
[24] Mann J B 1967 Atomic structure calculations *Los Alamos Science Laboratory Report* LA-3690
[25] Zarate E, Apell P and Echenique P M 1999 *Phys. Rev.* B **60** 2326
[26] Ziman J M 1972 *Principles of the Theory of Solids* (Cambridge: Cambridge University Press)
[27] Suarez C, Bron W E and Juhasz T 1995 *Phys. Rev. Lett.* **75** 4536
[28] Hohlfeld J, Müller J G, Wellershoff S S and Matthias E 1997 *Appl. Phys.* B **64** 387
[29] Hohlfeld J, Wellershoff S S, Güdde J, Conrad U, Jähnke V and Matthias E 2000 *Chem. Phys.* **251** 237
[30] Schmuttenmaer C A, Aeschlimann M, Elsayed-Ali H E, Miller R J D, Mantell D A, Cao J and Gao Y 1994 *Phys. Rev.* B **50** 8957
[31] Knoesel E, Hotzel A, Hertel T, Wolf M and Ertl G 1996 *Surf. Sci.* **368** 76
[32] Grimvall G 1981 *The Electron–Phonon Interaction in Metals (Selected Topics in Solid State Physics vol 16)* ed E P Wohlfahrt (Amsterdam: North-Holland)
[33] Knorren R, Bouzerar G and Bennemann K H 2001 *Phys. Rev.* B **63** 125122
[34] Aeschlimann M, Bauer M, Pawlik S, Knorren R, Bouzerar G and Bennemann K H 2000 *Appl. Phys.* A **71** 485
[35] Penn D R, Apell S P and Girvin S M 1985 *Phys. Rev.* B **32** 7753
[36] Pawlik S, Bauer M and Aeschlimann M 1997 *Surf. Sci.* **377–9** 206
[37] Cao J, Gao Y, Miller R J D, Elsayed-Ali H E and Mantell D A 1997 *Phys. Rev.* B **56** 1099
[38] Rosei R, Culp C H and Weaver J H 1974 *Phys. Rev.* B **10** 484